10.2514/6.2015-1222

AIAA SciTech Forum
5-9 January 2015, Kissimmee, Florida
53rd AIAA Aerospace Sciences Meeting

Multi-parameter estimation for spatially-resolved measurement of two-component velocity using absorption tomography

Mirko Gamba*

The University of Michigan, Department of Aerospace Engineering, Ann Arbor, MI 48109

In this work, we extend the use of absorption tomography typically used for the spatial measurement of species concentration and/or temperature over a planar region of a flow to the measurement of the local two-component velocity and potentially, simultaneously with temperature and pressure. The reconstruction is allowed by a compact reconstruction scheme based on the properties of the absorption lineshape (assumed to be a Voigt lineshape). Here, we will present the mathematical formulation of the problem, we will offer a possible solution strategy and we will demonstrate the method through a numerical experiment.

I. Introduction

LASER absorption spectroscopy (LAS) has now evolved into a robust diagnostic sensing scheme for a variety of flows. The general configuration for fluid flows and combustion applications is that of a line-of-sight (averaged) measurement of one or more state properties (pressure, temperature and/or species concentration) which are inferred from the radiation absorption characteristics along the path across the region of interest.[1] In practice, with reference to Fig 1a, this is achieved by shining a laser beam tuned to an absorption line across the region of interest, monitoring the fractional change of laser intensity across the line-of-sight (LOS), and inferring the sought quantity. Tunable diode lasers are typically used. Although different approaches have been developed,[2–7] here we focus on scanned-wavelength direct absorption measurements because it is most relevant to the work that will presented here.

II. Background

The amount of light absorbed by a medium along a path-length L where properties are uniform, can be described by the Beer-Lambert relation:

$$I_\nu = I_{\nu,o} e^{-\kappa_\nu L} \tag{1}$$

where κ_ν is the spectral absorption coefficient at a wavenumber ν (quantities with a subscript ν indicate spectral quantities). The term $I_\nu / I_{\nu,o}$ is the fractional change of laser intensity across the absorbing medium and it is what is measured. The spectral absorption coefficient is further expressed as:

$$\kappa_\nu = \chi p S(T) \phi(\nu); \tag{2}$$

where χ is mole fraction of the absorbing species, p is pressure, $S(T)$ is the linestrength of the transition line at temperature T, and $\phi(\nu)$ is the lineshape function (which depends on p and T due to broadening from molecular processes; pressure shift is here neglected). Under most conditions, the lineshape function can be approximated by a Voigt profile (convolution of a Gaussian and a Lorenzian function) and it is the result of the combined effect of collision-broadening (Lorenzian profile) and Doppler-broadening (Gaussian profile). The integral of κ_ν defines the integrated absorption coefficient A.

Assuming a Voigt profile, the lineshape of κ_ν depends on the primitive variables p and T. An alternative form is to reduce its description to the set of parameter a, σ and ν_o:[8] $\kappa_\nu(a, \sigma, \nu_o)$. Both descriptions are however equivalent as the parameters a and σ (a measures of the collisional and Doppler linewidths) are a function of p and T. In this regard, $\kappa_\nu(a, \sigma, \nu_o)$ contains all information about (p, T). Thus, a measure of (a, σ) could be used to directly extract a measure of (p, T). However, for temperature measurements, the more robust two-line ratiometric schemes are usually employed to infer T from the ratio of A measured for two different absorption lines.[9]

*Assistant Professor, Department of Aerospace Engineering, University of Michigan, AIAA Member.

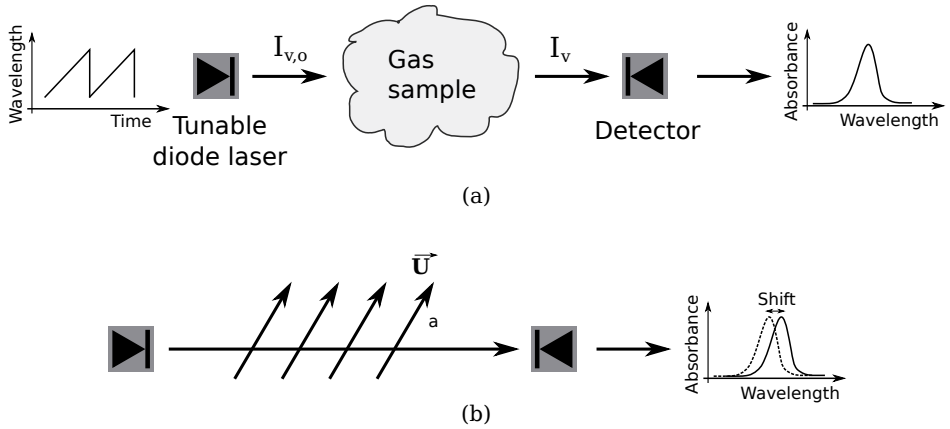

Figure 1: Schematic diagram of tunable diode laser absorption spectroscopy setup: (a) overall setup, (b) Doppler-shift velocimetry configuration.

The Doppler shift of the transition center line position ($\Delta\nu_s$) can also been used to infer the bulk-average, one-component velocity measurements.[3,10–14] The Doppler shift arises when the absorbing species move with a (bulk) velocity $\mathbf{U}$ in a direction with a relative angle α with respect to the measurement LOS:

$$\Delta\nu_s \sim |\mathbf{U}| \cos\alpha \tag{3}$$

See Fig 1b for a schematic diagram. We here neglect any other sources of shift in the center line position, such as pressure-induced shifts.

The typical sensor configuration for velocimetry and data processing is the same as for thermometry (Fig 1b). The difference is that the quantity of interest extracted from an absorption measurement is the shift in the absorption line-center, $\Delta\nu_s = \nu_{o,measured} - \nu_{o,nominal}$, and it is then related to the flow speed. The resulting velocity measurement is a LOS-average value, and thus the method applies when properties are uniform, and some knowledge of the flow direction (i.e., α) has to be known. Thus, velocimetry is usually applied to configurations where there exists a preferred bulk flow velocity in a principal direction.

The single-line implementation of LAS is valid only if flow properties are uniform. For non-uniform flows, one possible approach is the use of tomography to generate a spatial measurements of properties. Tomography has now found widespread applications in fluids and combustion applications. A discussion of the use of tomography in non-medical applications is described elsewhere.[15] The book by Herman[16] offers many details on computed tomography.

The main idea behind absorption tomography[17,18] (AT) is to gather measurements of the flow of interest using a set of laser beams oriented at different directions relative to each other. Each measurement generates an independent LOS measurement, or what is referred to as a "projection" P. The set of projections is then used to reconstruct the two-dimensional spatial distribution of the property of interest (typically temperature and/or concentration) over the plane defined by the set of projections. Traditionally, information along multiple lines is collected by using multiple simultaneous beams, by sweeping or traversing a beam across the measurement area, and replicating the measurement from different directions. Then, tomography reconstruction methods (like the ART method) are used to inferred the underlying field of interest. This approach typically leads to time-average properties due to the time needed to collect multiple projections. Some successful implementations of this method can be found in many references.[19–28] Tomography has however been used to infer only scalar quantities. How to develop a mathematical formulation to allow an implementation of the method for the measurement of non-scalar quantities (such as velocity) and/or for multiple quantities is the topic of this work.

In this work, we attempt at constructing a mathematical formulation of laser absorption based on the traditional Beer-Lambert relation, but that is capable of formulating the problem in a form that can by handled by tomography-like reconstruction approaches. Here we outline the method that has been developed so far and it will be demonstrated on a simple numerical example.

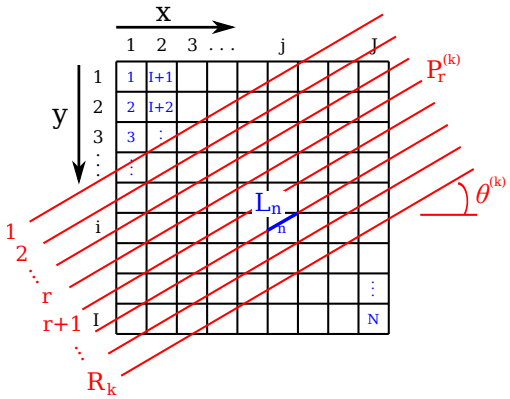

Figure 2: Schematic diagram of parallel-beam configuration in AT.

III. Mathematical formulation

A. Single-parameter formulation of tomography

Figure 2 shows a notional diagram of an AT setup over a non-uniform region. For convenience, we can here assume that all properties are uniform over the measurement region other than temperature, which is what we would like to infer from the measurements. The following is representative of existing methods. The measurement region is discretized in some fashion (a cartesian grid, for example, of elements $\{n = 1,...N\}$), over which properties (other than temperature) are assumed to be uniform over each element. We can refer to each element n as a pixel. A set of absorption projections $P_r^{(k)}$ is generated over discrete R laser beams. The subscript r refers to ray r, while the superscript (k) refers to a particular projection direction defined by the angle $\theta^{(k)}$ (relative to the $x-$axis, for example). For the reconstruction, multiple directions $\theta^{(k)}$, $\{k = 1,...K\}$, are required (each with R beams).

For this problem, the Beer-Lambert law governing the absorption process over each laser beam can be expressed in discretized form as:

$$P_{v,r}^{(k)} = \sum_{n=1}^{N} \kappa_{v,n} L_{r,n}^{(k)} \tag{4}$$

where $\kappa_{v,n} = \kappa_v(p, T_n)$, and $L_{r,n}^{(k)}$ is the chord-length of the r-th beam along the projection direction k subtended by the n-th pixel. $P_{v,r}^{(k)}$ is what would be measured. Note that Eq 4 and its terms have to be interpreted as spectral quantities (i.e., it is not a scalar value, but it is a quantity as a function of wavenumber). Thus, in a spectral view, $P_{v,r}^{(k)}$ is nothing more than a weighted sum of each spectral absorption coefficient at pixel n ($\kappa_{v,n}$) weighted by the path length subtended by each pixel along the LOS ($L_{r,n}^{(k)}$). Scanned direct absorption methods can be used to construct the problem in this form.

Because it is not necessary to work with spectral quantities (and we do not like it because it makes things less tractable), Eq 4 is further reduced by integrating the spectral projections and rewrite the problem in terms of integrated local absorption coefficients (A_n) and projections. This step reduces the problem to a more tractable scalar representation of unknowns A_n, which depends solely on the local temperature T_n:

$$P_r^{(k)} = \sum_{n=1}^{N} A_n L_{r,n}^{(k)} \tag{5}$$

Writing an equation of the type of Eq 5 for each ray in each projection direction, will then define a linear system of equations of the type $\mathbf{A}\underline{x} = \underline{b}$. The solution to this system will then produce the local value of A_n from which T_n can be extracted at each point n. Multi-line thermometry and concentration measurement approaches are mere extensions of single line methods in the context described here. In most applications, the number of rays and/or projections is limited, therefore Eq 5 is typically underdetermined and its solution requires some appropriate computed tomography reconstruction method.[15]

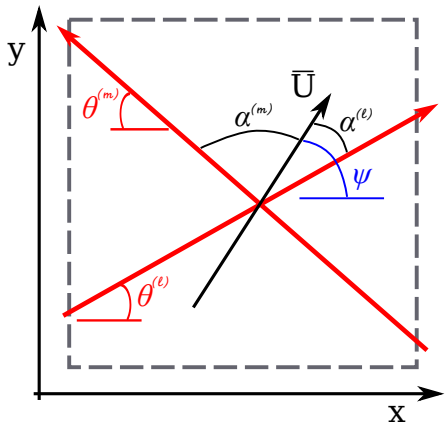

Figure 3: Schematic diagram of two-component LAS velocimetry.

B. Extension to multi-parameters, including two-components velocity

Consider now the case where multiple parameters are non-uniform on the measurement region and/or velocity is sought as well. Here we are primarily interested in the velocity field. First of all, note that extending the single beam configuration to the measurement of the Doppler shift, a two beam configuration could be used to extract the two components of velocity in the plane formed by the laser beams. Because each beam is subject to a different amount of Doppler shift (proportional to $|\mathbf{U}|\sin(\psi-\theta)$), if two beams are traveling in different directions, it is straightforward to show that by combining each measurement, it is possible to extract two velocity components (i.e., $|\mathbf{U}|$ and ψ). This is shown schematically in Fig 3 where two beams l and m propagating at (known) angles $\theta^{(l)}$ and $\theta^{(m)}$ (relative to the $x-$axis), probe a (uniform) flow with a bulk velocity $\mathbf{U}$ and direction ψ. Let us assume that the case shown in Fig 3 is representative of each pixel n in Fig 2.

In writing Eq 4, we noticed that each projection is the weighted sum of the spectral absorption coefficient. From our introductory discussion, all information about pressure, temperature and Doppler shift are enclosed in a local measure of $\kappa_{\nu,n}$. In particular, (p,T) can be inferred from the spectral profile, while $\mathbf{U}$ from the doppler shift. (Note, that here $\mathbf{U}$ should be interpreted as being only the in-plane 2C velocity of the true three-component field.) Note however, that in constructing this problem we have increased our number of unknown to four: p, T and $\mathbf{U}=(|\mathbf{U}|,\psi)$. Furthermore, there is an implicit dependance on the four parameters that cannot be simply decoupled as in the case only temperature is sought. This dependance is introduced by the fact that $\kappa_{\nu,n}$ becomes a function of θ through the Doppler shift and it differs (i.e., it is shifted) between different projection directions. Thus, we need to reduce the problem in a different form to resolve this limitation.

If we can assume that the local (i.e., at each pixel n) lineshape can be approximated by a Voigt profile, we can use the properties of Voigt profiles and the linearity of the absorption operator (Eq 1) to rewrite Eq 5 as:

$$\hat{\gamma}_{q,r}^{(k)} = \sum_{n=1}^{N} L_{r,n}^{(k)} \hat{\mu}_{q,rn}^{(k)} \tag{6}$$

where $\hat{\gamma}_{q,r}^{(k)}$ is the moment of order q of the Fourier transform of any $P_{\nu,r}^{(k)}$ and $\hat{\mu}_{q,rn}^{(k)}$ is the moment of order q of the Fourier transform of the local $\kappa_{\nu,n}^{(k)}$. Both $\hat{\gamma}_{q,r}^{(k)}$ and $\hat{\mu}_{q,rn}^{(k)}$ are now local scalar quantities of the corresponding spectral ones. We can then write an equation like Eq 6 for any moment of order q for the system of equations defined by $r=1,...R$ and $k=1,...K$ (i.e., for any ray and projection). In practice, we write the first M moments and thus we obtain a system of size $R\times K\times M$. Finally, it can be shown that the moments are a unique representation of the parameters $(a,\sigma,\Delta\nu_s)$, thus a solution of Eq 6 allows us to reconstruct these three parameters and thus $(p,T,|\mathbf{U}|,\psi)$, at each pixel. This is shown with a numerical example.

IV. Numerical example

To show the method, the following simple numerical example is constructed. The example is based on a geometry, configuration and discretization as shown in Fig 2. An arbitrary distribution of pressure, temperature and in-plane

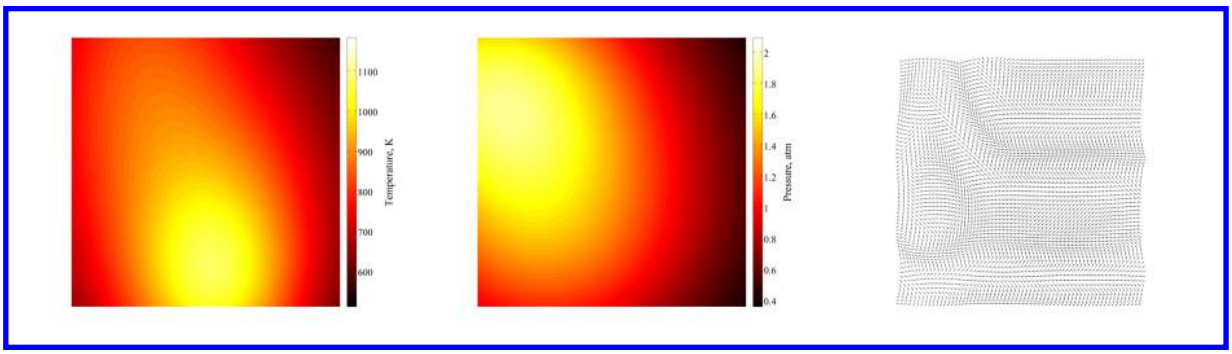

(a)

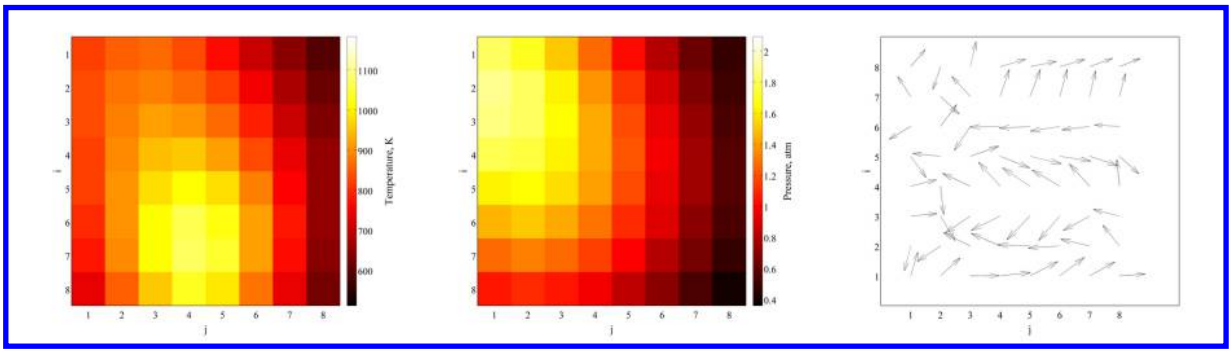

(b)

Figure 4: (a) Exact spatial distribution of temperature T (left), pressure p (middle) and in-plane two-component velocity $(|\mathbf{U}|, \psi)$ (right) of target field (phantom field). (b) Resampled phantom on a 8×8 grid – these are the distributions to be reconstructed from projections.

two-component velocity was assumed and it is shown in Fig 4. For representation purposes, Fig 4a shows the exact distribution on a fine grid. However, for demonstration purposes and for an initial assessment of the method, a resampled representation on a coarse grid is used. Figure 4b shows the resampled distribution over an 8×8 grid. This latter set of distribution is the initial point of the numerical analysis. In all effects, these distributions are the phantoms of the reconstruction process. For consistency in the reconstruction process, the domain is discretized in a 8×8 grid ($N = 64$) from which projections are constructed over 4 different directions ($K = 4$), each with 16 beams ($R = 16$). We used the first 3 moments ($M = 3$). Absorption was assumed to be for an H_2O transition near 7205.246 cm^{-1} (spectroscopy data taken from Liu et al.[29]) where a uniform distribution of water was assumed for simplicity (otherwise it would be a 5th parameter to estimate from the reconstruction process). With reference to Fig 4, note that pressure was taken to span across the domain from 0.5 atm to 1.5 atm; temperature from 600 K to 1100 K; velocity to vary from 400 to 700 m/s (with associated line-center shift in the range $0.001 - 0.01$ cm^{-1}); $\chi = 1$ throughout.

Given the target initial distributions (phantoms) of $(p, T, |\mathbf{U}|, \psi)$, $\kappa_{\nu,n}$ were first computed for each beam, direction and n combination, and then the corresponding projections were computed. This was the starting point of the reconstruction method and simulates what a measurement would provide. The solution of the resulting system of equations was achieved using a recursive ART algorithm where each projection was solved independently (for the local moments of the local Voigt profiles), velocity information was extracted from two projections, and the results combined to provide an initial guess to the following step in the recursive process. Pressure and temperature were also reconstructed at each step. The process was repeated until the (spatial median) error on 3 of the 4 parameters $(p, T, |\mathbf{U}|, \psi)$, $\kappa_{\nu,n}$ was less than 1% (this choice is arbitrary made to speed up convergence to a final solution for demonstration purposes). In this example the error was computed as the local difference between the reconstructed and true values (i.e., Fig 4b) of each of the four quantities of interest.

Starting from the projections, the local moments of (the Fourier transform of) $\kappa_{\nu,n}$, and thus $\kappa_{\nu,n}$ itself, were reconstructed. An example of the reconstructed local $\kappa_{\nu,n}$ are shown in Fig 5 (red dash line) along with the exact initial profile (black solid line) at one intermediate iteration (after 20 cycles) before convergence to a final solution was achieved. A qualitative comparison between the exact and reconstructed $\kappa_{\nu,n}$ can give a qualitative indication of

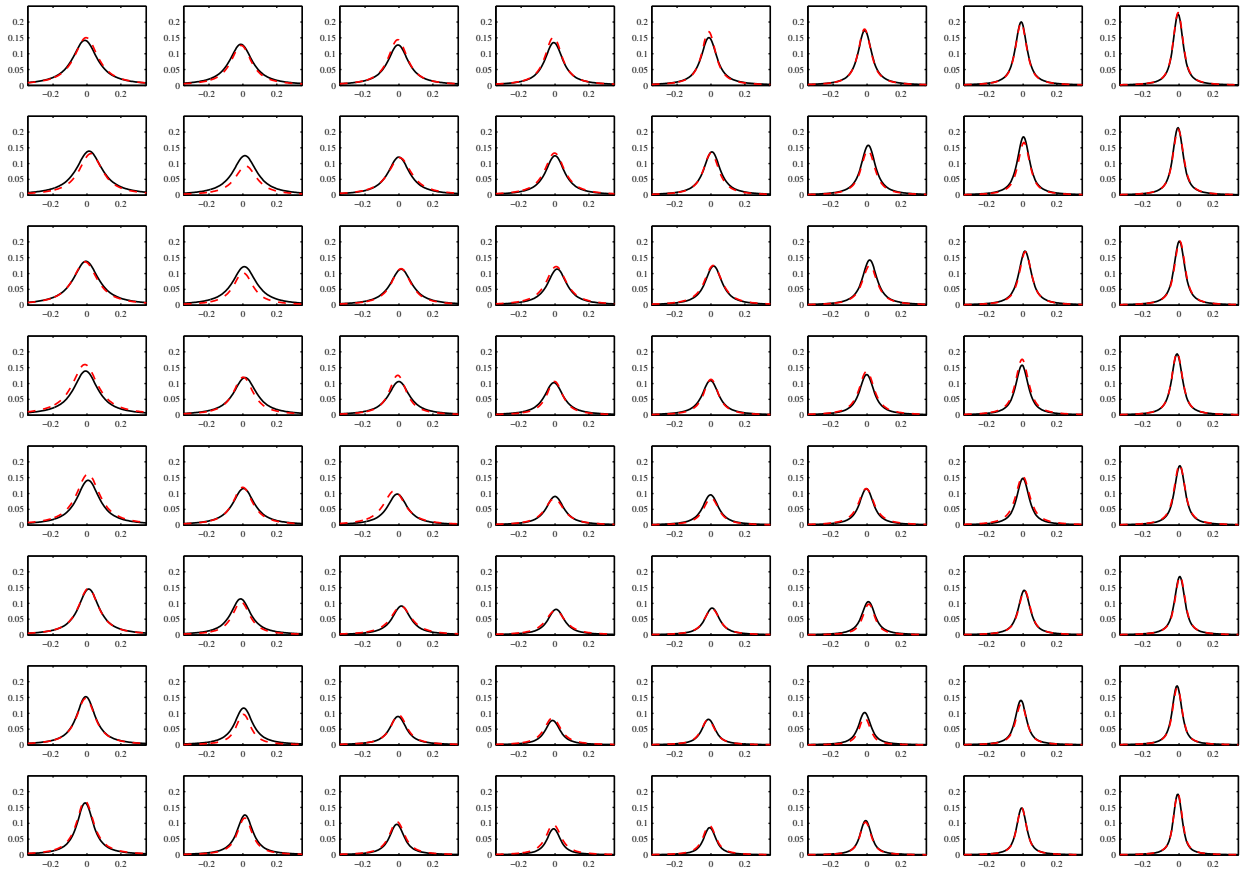

Figure 5: Exact (solid black line) and reconstructed (red dash line) $\kappa_{\nu,n}$ at one intermediate iteration (before convergence to a final solution was achieved): each plot refers to $\kappa_{\nu,n}$ in each of the 8×8 pixels ($i-j$ ordering as used in Fig 4) and represents the combined local contribution of the local $(p, T, |\mathbf{U}|, \psi)$, $\kappa_{\nu,n}$ to $\kappa_{\nu,n}$. The x-axis is $\nu - \nu_o$.

the difference between the true values of the primitive variables $(p, T, |\mathbf{U}|, \psi)$: the closer the two $\kappa_{\nu,n}$ are, the closer are the corresponding aerothermodynamic states they represent. We can thus observe that in certain locations of the phantom we reconstruct $\kappa_{\nu,n}$ fairly well, but in many locations the two differ significantly. However, as the iteration progresses, the reconstructed $\kappa_{\nu,n}$ tends to the exact one.

To summarize the converge to the exact solution, Fig 6 shows the error in the reconstructed properties $(p, T, |\mathbf{U}|, \psi)$ after inverting $\kappa_{\nu,n}$ as a function of iteration number. For this simplified example, a final solution to within 1% of the true value (in a median sense) was recovered after about 300 cycles. We can observe that different properties converge to the true solution at different rates. For example, the algorithm converges to the true value of temperature fairly quickly. Pressure also tends to converge faster than the velocity terms. In this example we observe that the quantity that is less accurate is speed. In general, it was observed that either ψ or $|\mathbf{U}|$ are the quantities that limit convergence. We can also observe that the convergence does not have a constant rate. In fact, the convergence rate is very fast initially, but it significantly slows down afterwords. The overall errors could be decreased further than what observed here by increasing the number of iterations. After some point, however, the convergence rate becomes very slow. Another observation is that during the iteration process the (median) error was observed to increase momentary, and then recover. The exact reason for this behavior is currently not known, but it is most likely due to the fairly crude iterative process being considered at this point. Further improvements of the solution schemes are in fact needed to improve convergence of the reconstruction method. It was however clear that this process was initiated by obtaining a large local error (e.g., at one pixel) somewhere in the reconstructed field, which then propagated to other pixels in subsequent iterations. The solution was however able to recover after some iterations.

The reconstructed fields $(p, T, |\mathbf{U}|, \psi)$ at the end of the iteration process are shown in Fig 7. For the in-plane velocity components, the figure shows both the reconstructed components (red vectors) and the true components (black vectors) for a more direct comparison. For the pressure and temperature fields, Fig 4 can be referred to. Overall, the

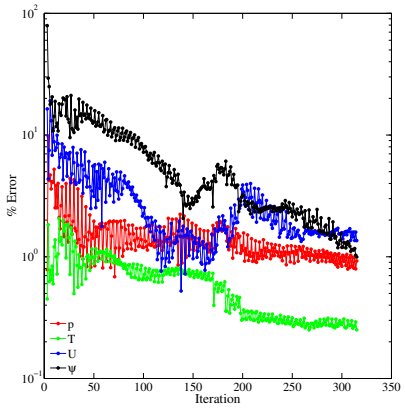

Figure 6: Reconstruction error of $p, T, |\mathbf{U}|, \psi$ as a function of iteration.

qualitative distribution of all quantities of interest have been reconstructed satisfactorily. To be more specific, the spatial distributions of the (percentage) error, defined as the difference between reconstructed and true value (relative to the true value), for some of the quantities of interest $(p, T, |\mathbf{U}|)$ are shown in Fig 8. In general, the errors in p and T are limited to a few percent, while larger percentage errors are observed for the speed (and similarly for Ψ). Even though the methodology appears promising, the method and its implementation still requires many improvements to attempt at reducing the discrepancy further. Note, however, that as introduced above, if more iterations are considered, the various errors do tend to decrease (although at a slowing rate). To conclude, numerical tests over larger systems have also been conducted (up to $N = 15 \times 15$ using only 4 projection directions). However, as the size of the problem increased, the accuracy of the solution significantly degraded (relative errors as large as 50% have been observed).

V. Conclusions and outlook

We have here presented the use of AT with a compact representation of the absorption process to write a system of equations that captures the dependance of multi-parameters $(p, T, |\mathbf{U}|, \psi)$ to be used in a tomography reconstruction method to infer a local measure of the in-plane two-component velocity along with temperature and pressure. Here a brief view of the mathematical model is given. The method is also demonstrated with a simple numerical example. The method appears to be capable of describing the problem and providing a reconstruction methodology in these well-defined simple numerical experiment. However, much work is needed to improve the overall methodology, the mathematical representation, and the numerical implementation of the method before more realistic situations can be considered. In particular, it is now clear that one of the limitations is the implementation of a more robust reconstruction algorithm. In the numerical experiment presented here the reconstruction algorithm was based on a sequential use of the ART method where velocity information was extracted from applying ART to two independent set of projections. Furthermore, during the iterative process, no intermediate vector validation scheme was used (as one might do in particle image velocimetry), which could improve the convergence, for example by removing outliers that could contaminate the entire solution in subsequent iterations (as observed in this numerical experiment). At this stage the method is still in its infancy. It will require much more development and testing over more complex and realistic configurations. The importance of the new method proposed here is that it will enable the estimation of multiple parameters, and in particular a 'spatially resolved' measurement of the two-component velocity in flows without the need of tracer particles like in particle image velocimetry.

Acknowledgments

This paper is based on work supported by the Air Force Office of Scientific Research under Grant No. FA9550-14-1-0396 with Dr. Chiping Li as Technical Monitor.

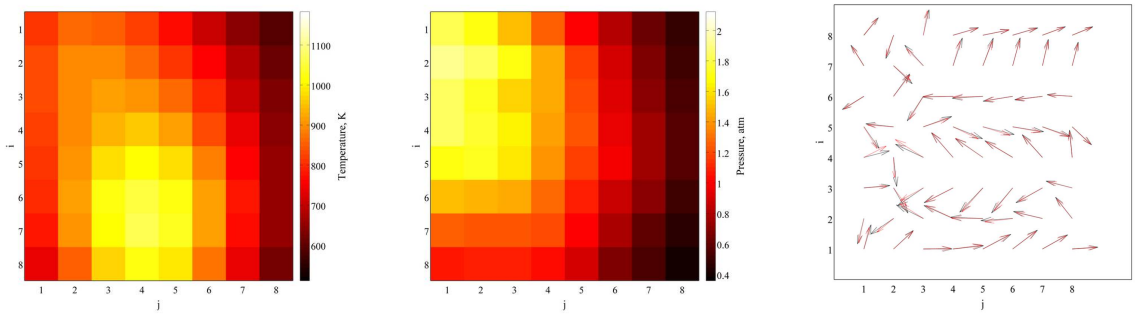

Figure 7: Reconstructed spatial distribution of temperature T (left), pressure p (middle) and in-plane two-component velocity $(|\mathbf{U}|, \psi)$ (right) of the phantom field. For the velocity field, both exact and reconstructed vectors are presented; in particular: black vectors indicate exact field, while the red vectors indicate the reconstructed field.

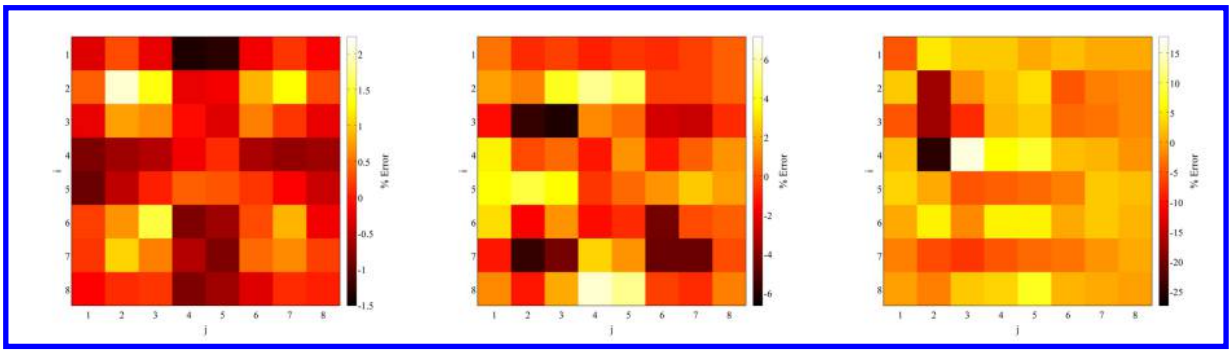

Figure 8: Spatial distribution of the reconstruction error in temperature T (left), pressure p (middle) and speed $|\mathbf{U}|$ (right) of the phantom field.

References

[1]Allen, M. G., "Diode laser absorption sensors for gas-dynamics and combustion flows," *Meas. Sci. Technol.*, Vol. 9, 1998, pp. 545–562.

[2]Reid, J. and Labrie, D., "Second-harmonic detection with tunable diode lasers - comparison of experiments and theory," *Appl. Physics B: Lasers and Optics*, Vol. 26, No. 203-210, 1981.

[3]Philippe, L. C. and Hanson, R. K., "Laser diode wavelength-modulation spectroscopy for simultaneous measurement of temperature, pressure, and velocity in shock-heated oxygen flows," *Appl. Optics*, Vol. 32, No. 30, 1993, pp. 6090–6103.

[4]Liu, J. T. C., Jeffries, J. B., and Hanson, R. K., "Wavelength modulation absorption spectroscopy with 2 f detection using multiplexed diode lasers for rapid temperature measurements in gaseous flows," *Appl. Physics B: Lasers and Optics*, Vol. 78, No. 3-4, 2004, pp. 503–511.

[5]Farooq, A., Jeffries, J. B., and Hanson, R. K., "Measurements of CO2 concentration and temperature at high pressures using 1f-normalized WMS-2f spectroscopy near 2.7 μm," *Appl. Optics*, Vol. 48, No. 35, 2009, pp. 6740–6753.

[6]Rieker, G. B., Jeffries, J. B., and Hanson, R. K., "Calibration-free wavelength-modulation spectroscopy for measurements of gas temperature and concentration in harsh environments," *Appl. Optics*, Vol. 48, No. 29, 2009, pp. 5546–5560.

[7]Farooq, A., Jeffries, J. B., and Hanson, R. K., "Sensitive detection of temperature behind reflected shock waves using wavelength modulation spectroscopy of CO_2 near 2.7 μm," *Appl. Physics B: Lasers and Optics*, Vol. 96, No. 1, 2009, pp. 161–173.

[8]Armstrong, B. H., "Spectrum line profiles: the Voigt function," *Journal of Quantitative Spectroscopy and Radiative Transfer*, Vol. 7, 1967, pp. 61–88.

[9]Arroyo, M. P. and Hanson, R. K., "Absorption measurements of water-vapor concentration, temperature, and line-shape parameters using tunable InGaAsP diode laser," *Appl. Optics*, Vol. 32, No. 30, 1993, pp. 6104–6116.

[10]Arroyo, M. P., Langlois, S., and Hanson, R. K., "Diode-laser absorption technique for simultaneous measurements of multiple gasdynamic parameters in high-speed flows containing water vapor," *Appl. Optics*, Vol. 33, No. 15, 1994, pp. 3296–3307.

[11]Miller, M. F., Kessler, W. J., and Allen, M. G., "Diode laser-based air mass flux sensor for subsonic aeropropulsion inlets," *Appl. Optics*, Vol. 35, No. 24, 1996, pp. 4905–4912.

[12]Williams, S., Barone, D., Barhorst, T., Jackson, K., Lin, K. M., Masterson, P., Zhao, Q., and Sappey, A. D., "Diode laser diagnostics for high speed flows," *14th AIAA/AHI Space Planes and Hypersonic SYstems and Technologies Conference, Paper No AIAA-2006-7999*, 2006.

[13]Lyle, K. H., Jeffries, J. B., and Hanson, R. K., "Diode-laser sensor for air-mass flux 1: design and wind-tunnel validation," *AIAA J.*, Vol. 45, No. 9, 2007.

[14]Chang, L. S., *Development of a diode laser sensor for measurement of mass flux in supersonic flow*, Ph.D. thesis, Stanford University, 2011.

[15]Verhoeven, D., "Limited-data computed tomography algorithms for the physical sciences," *Appl. Optics*, Vol. 32, No. 20, 1993.

[16]Herman, G. T., *Fundamentals of Computerized Tomography: Image Reconstruction from Projections*, Springer Berlin / Heidelberg, 2009.

[17]Emmerman, P. J., Goulard, R., Santoro, R. J., and Semerjian, H. G., "Multiangular absorption diagnostics of a turbulent Argon-Methane jet," *J. Energy*, Vol. 4, No. 2, 1980, pp. 70–77.

[18]Santoro, R. J., Semerjian, H. G., Emmerman, P. J., and Goulard, R., "Optical tomography for flow field diagnostics," *Int. J. Heat Mass Transfer*, Vol. 24, No. 7, 1981, pp. 1139–1150.

[19]Gillet, B., Hardalupas, Y., Kavounides, C., and Taylor, A. M. K. P., "Infrared absorption for measurement of hydrocarbon cancontration in fuel/air mixtures (mast-b-liquid)," *Applied Thermal Engineering*, Vol. 24, 2004, pp. 1633–1653.

[20]Lindstrom, C., Tam, C.-J., Davis, D., Eklund, D., and Williams, S., "Diode laser absortion tomography of 2D supersonic flow," *43rd AIAA/ASME/SAE/ASEE Joint Propulsion Conference and Exhibit, Paper No. AIAA-2007-5014*, 2007.

[21]Bryner, E., *Development of Tunable Diode Laser Absorption Tomography for Determination of Spatially Resolved Distributions of Water Vapor Temperature and Concentration*, Ph.D. thesis, University of Virginia, 2010.

[22]Wang, F., Cen, K. F., Li, N., Jeffries, J. B., Huang, Q. X., Yan, J. H., and Chi, Y., "Two-dimensional tomography for gas concentration and temperature distributions based on tunable diode laser absorption spectroscopy," *Meas. Sci. Technol.*, Vol. 21, 2010, pp. 045301.

[23]Bryner, E., Busa, K., McDaniel, J. C., Goyne, C. P., and Diskin, G. S., "Spatially resolved temperature and water vapor concentration distributions in a flat flame burner by tunable diode laser absorption tomography," *49th AIAA Aerospace Science Meeting, Paper No. AIAA-2011-1291*, 2011.

[24]Kasyutich, V. and Martin, P., "Towards a two-dimensional concentration and temperature laser absorption tomography sensor system," *Appl. Physics B: Lasers and Optics*, Vol. 102, 2011, pp. 149–162.

[25]Song, J., Hong, Y., Wang, G., and Pan, H., "Algebraic tomographic reconstruction of two-dimensional gas temperature based on tunable diode laser absorption spectroscopy," *Appl. Physics B: Lasers and Optics*, 2013, pp. 1–9.

[26]Ma, L. and Cai, W., "Numerical investigation of hyperspectral tomography for simultaneous temperature and concentration imaging," *Appl. Optics*, Vol. 47, No. 21, 2008, pp. 3751–3759.

[27]Ma, L., Cau, W., Caswell, A. W., Kraetschmer, T., Sanders, S. T., Roy, S., and Gord, J. R., "Tomographic imaging of temperature and chemical species based on hyperspectral absorption spectroscopy," *Optics Express*, Vol. 17, No. 10, 2009.

[28]An, X., Kraetschmer, T., Takami, K., Sanders, S. T., Ma, L., Cai, W., Li, X., Roy, S., and Gord, J. R., "Validation of temperature imaging by H_2O absorption spectroscopy using hyperspectral tomography in controlled experiments," *Appl. Optics*, Vol. 50, No. 4, 2011, pp. A29–A37.

[29]Liu, X., Jeffries, J. B., and Hanson, R. K., "Measurements of spectral parameters of water vapor transitions near 1388 and 1345 nm for accurate simulation of high-pressure absorption spectra," *Meas. Sci. Technol.*, Vol. 18, 2007, pp. 1185–1194.